A continuous homogenized model for the dynamical analysis of rotationally periodic structures with imperfections

Paolo Bisegna[1], Giovanni Caruso[2]
[1] *Department of Civil Engineering, University of Rome Tor Vergata, Italy*
E-mail: bisegna@uniroma2.it

[2] *ITC-CNR, Italy*
E-mail: g.caruso@ing.uniroma2.it

Keywords: Rotationally periodic structures, vibration localization, frequency split, homogenization technique, perturbation analysis.

SUMMARY. Rotationally periodic structures, like turbines, bladed disks, stators and rotors of electric machineries or satellite antennae, play an important role in many fields of the technology. It is well known that when even small structural imperfections are present, destroying the perfect periodicity of the structure, each couple of degenerate modal frequencies splits into two different values (mistuning) and the corresponding modal shapes exhibit peaks of vibration amplitude (localization phenomenon). In this paper a continuous model describing the in-plane vibrations of an imperfect bladed rotor is derived via the homogenization theory, and is applied to the analysis of the localization phenomenon. Imperfections are modeled as perturbations of mass and bending stiffness of some blades, and a perturbation approach is adopted in order to find out the split eigenfrequencies and eigenmodes of the imperfect structure. Numerical simulations show that the proposed model is suitable and effective for the identification and analysis of the localization phenomenon, requiring much lower computational effort than classical finite element models.

1 INTRODUCTION

Rotationally periodic structures are composed of a number N_b of identical substructures, periodically arranged around an axis, so that the original shape is recovered upon rotations of an angle of $2\pi/N_b$ radiants. This typology of structures plays an important role in many engineering applications, such as turbines, cooling towers with legs, satellite antennae, stator-rotor assemblies of electrical machineries, and so on. It is well known that, due to the periodicity they posses, these structures exhibit couples of degenerate eigenmodes at the same eigenfrequency [Thomas, 1979, Shen, 1994]. Finite element analysis has been extensively used [Thomas, 1979, Cai et al., 1990, Fricker and Potter, 1981] in order to study the free and forced response of perfect rotationally periodic structures. By exploiting their periodicity properties, it is possible to obtain a discrete model of the structure by considering just a single substructure and enforcing suitable constraints. Indeed, for a given structural eigenmode, all the substructures exhibit the same vibration amplitude with different phases.

When imperfections are present, destroying the symmetry of the structure, the degeneracy is removed and each couple of eigenmodes belonging to the same eigenfrequency in the perfect case, splits into two non-degenerate eigenmodes at different frequencies. Moreover, some eigenmodes exhibit the well known localization phenomenon [Sinha, 1986, Pierre and Dowell, 1987], consisting of a local increase of vibration amplitude, which is dangerous because it may lead to fatigue failure of the structure. This phenomenon has been extensively studied in the literature by means of finite element models [Huang, 2006, Chiu and Huang, 2007] or simplified discrete models [Tang and Wang, 2003,

Yoo et al., 2003, Fang et al., 2006]. The finite element approach is accurate, since it can model the exact geometry of the structure, but it requires a high computational effort; indeed, due to the presence of imperfections, the whole structure need to be discretized. The simplified models describe the blades as lumped masses and the coupling between adjacent blades is accounted for by the presence of elastic springs. Although these models are computationally more efficient than finite element schemes, they are able to describe the influence of imperfections on the rotor dynamics only in a qualitative way, since they are based on a simplified geometry, quite different from the actual rotor geometry. Continuous models are less developed in the literature; an attempt has been done in [Wagner and Griffin, 1993], where a perfect structure is considered, composed of grouped blades mounted on a flexible disk; the coupling between adjacent groups of blades, due to presence of the flexible disk, is modeled by means of discrete springs, whereas the stiffness of the blades is accounted for by using distributed springs.

In real situations, each blade is coupled to all the other blades mounted on the flexible disk trough the disk itself, and this feature should be taken into account for an accurate evaluation of the structural eigenmodes and eigenfrequencies. In this paper, a model of a bladed rotor is derived via the homogenization theory, and is applied to the investigation of the localization phenomenon in imperfect bladed rotors. The considered structure is composed of N_b elastic blades clamped to an elastic ring, modeling the rotor disk. The presence of imperfections is accounted for by perturbing the linear mass density and the bending stiffness of the imperfect blades. The homogenization technique is employed in order to obtain a continuous model of the structure: the blade dynamical behavior is described by the Euler-Bernoulli vibrating beam equation, equipped with suitable boundary conditions, taking into account the presence of the elastic ring which couples all the blades together. A perturbation technique is adopted to obtain a linearized variational formulation, whose solution supplies the modal split eigenfrequencies and eigenmodes of the imperfect rotor. Numerical simulations reveal the frequency split effect and the localization phenomenon due to the presence of imperfections, showing the ability of the proposed model to investigate the dynamics of imperfect turbine bladed rotors. Due to its accuracy and efficiency, the proposed homogenized model seems to be a useful tool for the design and the parametric analysis of rotationally periodic structures.

2 HOMOGENIZED MODEL

In this section a homogenized model for the analysis of the in-plane vibrations of a bladed rotor is developed. The rotor is schematically represented in fig. 1; it is made of a linearly elastic material and is composed of N_b blades, of length l_b, clamped on a ring of radius R, representing the turbine shaft. The angular spacing $\delta\theta_o$ between any two adjacent blades is constant and equal to $2\pi/N_b$.

2.1 Euler-Bernoulli model

In order to develop the homogenized model, a classical model based on the Euler-Bernoulli theory is first recalled, denoted in the foregoing with the acronym EB. A polar coordinate system (O, ρ, θ) is introduced. Let $u(\theta)$, $w(\theta)$ be the tangential and radial displacement of the ring, respectively; let $U_i(\rho)$, $W_i(\rho)$ be the transversal and axial displacement of the i^{th} blade, placed at an angle θ_i, respectively, as shown in fig. 1. Both the ring and the blades are assumed to be inextensible. As well known, the axial strain ε, the rotation φ and the variation of curvature $\Delta\chi$ of the cross section of the ring are respectively given by

$$\varepsilon = \frac{1}{R}\left(\frac{\partial u}{\partial \theta} + w\right), \qquad \varphi = \frac{1}{R}\left(u - \frac{\partial w}{\partial \theta}\right), \qquad \chi = \frac{1}{R^2}\left(\frac{\partial u}{\partial \theta} - \frac{\partial^2 w}{\partial \theta^2}\right) \tag{1}$$

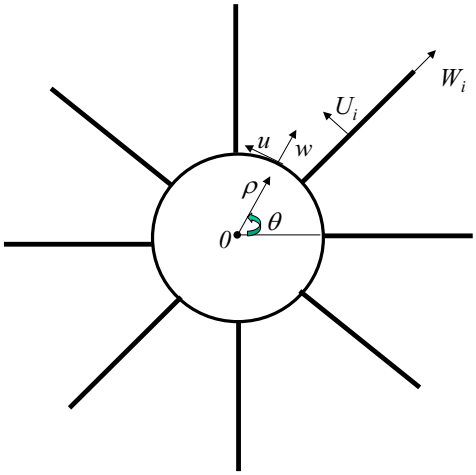

Figure 1: Schematization of a bladed rotor

where R is the ring radius. Let assume for now that no imperfections are present, and let σ_r and K_r denote, respectively, the linear mass density and in-plane bending stiffness of the ring, which are constant quantities. Moreover let σ_{ob} and K_{ob} denote, respectively, the linear mass density and bending stiffness of each blade, possibly depending on the radial variable ρ. The Hamiltonian functional governing the dynamical behavior of the structure is given by

$$\mathcal{H} = \frac{1}{2}\int_0^{2\pi} \sigma_r \left[\left(\frac{\partial u}{\partial t}\right)^2 + \left(\frac{\partial w}{\partial t}\right)^2\right] R\, d\theta + \frac{1}{2}\sum_{i=1}^{N_b}\int_R^{R+l_b} \sigma_{ob}(\rho)\left[\left(\frac{\partial U_i}{\partial t}\right)^2 + \left(\frac{\partial W_i}{\partial t}\right)^2\right] d\rho$$
$$- \frac{1}{2}\int_0^{2\pi} \frac{K_r}{R^4}\left(\frac{\partial u}{\partial \theta} - \frac{\partial^2 w}{\partial \theta^2}\right)^2 R\, d\theta - \frac{1}{2}\sum_{i=1}^{N_b}\int_R^{R+l_b} K_{ob}(\rho)\left(\frac{\partial^2 U_i}{\partial \rho^2}\right)^2 d\rho \quad (2)$$

subjected to the following constraints

$$\frac{1}{R}\left(\frac{\partial u}{\partial \theta} + w\right) = 0, \quad \theta \in (0, 2\pi); \qquad \frac{\partial W_i}{\partial \rho} = 0, \quad \rho \in (R, R + l_b), \quad i = 1 \dots N_b;$$
$$W_i = w, \quad U_i = u, \quad \frac{\partial U_i}{\partial \rho} = \frac{1}{R}\left(u - \frac{\partial w}{\partial \theta}\right), \quad \rho = R,\ \theta = \theta_i,\ i = 1 \dots N_b \quad (3)$$

where t denotes the time. Let now assume that the j^{th} rotor blade, placed at an angle θ_j, is imperfect. A great variety of imperfections can be accounted for by suitably modifying the linear mass density and/or the bending stiffness of a single blade, e.g. in [Fang et al., 2006] a crack in a blade is modeled by suitably reducing the bending stiffness of the damaged blade. Accordingly, the linear mass density $\sigma_{bj}(\rho)$ and bending stiffness $K_{bj}(\rho)$ of the imperfect j^{th} blade are represented as follows

$$\sigma_{bj}(\rho) = \sigma_{ob}(\rho) + \delta\sigma_{bj}(\rho), \qquad K_{bj}(\rho) = K_{ob}(\rho) + \delta K_{bj}(\rho) \quad (4)$$

where $\delta\sigma_{bj}$ and δK_{bj} are the variations with respect to their corresponding nominal values.

2.2 Homogenized model for a perfect rotor

In order to derive a homogenized model for the dynamical behavior of a bladed rotor, let assume for now that no imperfections are present. The variational formulation (2) is rewritten for a family of rotors with increasing number N of blades, starting from $N = N_b$, which is the number of blades exhibited by the reference rotor, in order to approach the homogenization limit $N \to \infty$. It is assumed that, for each chosen N, the blade linear mass density σ_{ob}^N rescales as $\sigma_{ob}(\rho)\frac{N_b}{N}$ and the blade bending stiffness K_{ob}^N rescales as $K_{ob}(\rho)\frac{N_b}{N}$, such that the overlined quantities

$$\overline{\sigma}_{ob}(\rho) = \frac{\sigma_{ob}^N}{\delta\theta}, \qquad \overline{K}_{ob}(\rho) = \frac{K_{ob}^N}{\delta\theta} \tag{5}$$

with $\delta\theta = 2\pi/N$ being the angular spacing between adjacent blades, do not depend on N. The quantities defined in (5) represent, respectively, the homogenized linear mass density and bending stiffness. These assumptions are substituted into the functional (2) and the homogenization limit $N \to \infty$ is then performed; by extending the functions $U_i(\rho)$ and $W_i(\rho)$, $i = 1 \dots N$, to the annular region $(R, R + l_b) \times (0, 2\pi)$ and assuming that they strongly converge, together with their derivatives, to functions $U(\rho, \theta)$ and $W(\rho, \theta)$, it is possible to prove that the functional (2), for $N \to \infty$, converges to

$$\begin{aligned}\mathcal{H}_{hom} = \frac{1}{2}\int_0^{2\pi} \sigma_r \left[\left(\frac{\partial u}{\partial t}\right)^2 + \left(\frac{\partial w}{\partial t}\right)^2\right] R\, d\theta + \frac{1}{2}\int_0^{2\pi}\int_R^{R+l_b} \overline{\sigma}_{ob}(\rho)\left[\left(\frac{\partial U}{\partial t}\right)^2 + \left(\frac{\partial W}{\partial t}\right)^2\right] d\rho d\theta \\ - \frac{1}{2}\int_0^{2\pi} \frac{K_r}{R^4}\left(\frac{\partial u}{\partial \theta} - \frac{\partial^2 w}{\partial \theta^2}\right)^2 R\, d\theta - \frac{1}{2}\int_0^{2\pi}\int_R^{R+l_b} \overline{K}_{ob}(\rho)\left(\frac{\partial^2 U}{\partial \rho^2}\right)^2 d\rho d\theta\end{aligned} \tag{6}$$

subjected to the following constraints

$$\begin{aligned}&\frac{1}{R}\left(\frac{\partial u}{\partial \theta} + w\right) = 0, \quad \theta \in (0, 2\pi); \qquad \frac{\partial W}{\partial \rho} = 0, \quad (\rho, \theta) \in (R, R + l_b) \times (0, 2\pi); \\ &W = w, \quad U = u, \quad \frac{\partial U}{\partial \rho} = \frac{1}{R}\left(u - \frac{\partial w}{\partial \theta}\right), \quad \rho = R,\ \theta \in (0, 2\pi)\end{aligned} \tag{7}$$

obtained from (3) after performing the homogenization limit. By a priory enforcing the constraints (7) in (6), the following functional is obtained

$$\begin{aligned}\mathcal{H}_{hom} = \frac{1}{2}\int_0^{2\pi} \sigma_r \left[\left(\frac{\partial U}{\partial t}\right)^2 + \left(-\frac{\partial^2 U}{\partial \theta \partial t}\right)^2\right]_{\rho=R} R\, d\theta + \frac{1}{2}\int_0^{2\pi}\int_R^{R+l_b} \overline{\sigma}_{ob}(\rho)\left(\frac{\partial U}{\partial t}\right)^2 d\rho d\theta \\ + \frac{1}{2}\int_0^{2\pi}\left(\int_R^{R+l_b} \overline{\sigma}_{ob}(\rho)\, d\rho\right)\left[-\frac{\partial^2 U}{\partial \theta \partial t}\right]_{\rho=R}^2 d\theta - \frac{1}{2}\int_0^{2\pi} \frac{K_r}{R^4}\left[\frac{\partial U}{\partial \theta} + \frac{\partial^3 U}{\partial \theta^3}\right]_{\rho=R}^2 R\, d\theta \\ - \frac{1}{2}\int_0^{2\pi}\int_R^{R+l_b} \overline{K}_{ob}(\rho)\left(\frac{\partial^2 U}{\partial \rho^2}\right)^2 d\rho d\theta\end{aligned} \tag{8}$$

subjected to the essential constraint condition

$$\frac{\partial U}{\partial \rho} = \frac{1}{R}\left(U + \frac{\partial^2 U}{\partial \theta^2}\right), \qquad \rho = R,\ \theta \in (0, 2\pi) \tag{9}$$

In order to study the free vibrations of the perfect bladed rotor, a sinusoidal time dependence of the unknown U is assumed (i.e., with a slightly abuse of notation, $U(\rho,\theta,t) = U(\rho,\theta)e^{i\omega\, t}$), i being here the imaginary unit. Enforcing this position and recasting the functional (8) into a variational form, it is obtained

$$
\begin{aligned}
-\omega^2\Big\{ \int_0^{2\pi} \sigma_r \left[U\psi + \frac{\partial U}{\partial\theta}\frac{\partial\psi}{\partial\theta}\right]_{\rho=R} R d\theta + \int_0^{2\pi}\int_R^{R+l_b} \overline{\sigma}_{ob}(\rho) U\psi \, d\rho d\theta \\
+\int_0^{2\pi}\left(\int_R^{R+l_b} \overline{\sigma}_{ob}(\rho)\, d\rho\right)\left[\frac{\partial U}{\partial\theta}\frac{\partial\psi}{\partial\theta}\right]_{\rho=R} d\theta\Big\} + \int_0^{2\pi}\frac{K_r}{R^4}\left[\left(\frac{\partial U}{\partial\theta}+\frac{\partial^3 U}{\partial\theta^3}\right)\left(\frac{\partial\psi}{\partial\theta}+\frac{\partial^3\psi}{\partial\theta^3}\right)\right]_{\rho=R} R\, d\theta \\
+\int_0^{2\pi}\int_R^{R+l_b} \overline{K}_{ob}(\rho)\frac{\partial^2 U}{\partial\rho^2}\frac{\partial^2\psi}{\partial\rho^2}\, d\rho d\theta = 0 \qquad (10)
\end{aligned}
$$

subjected to the following constraints

$$
\frac{\partial U}{\partial\rho} = \frac{1}{R}\left(U + \frac{\partial^2 U}{\partial\theta^2}\right), \qquad \frac{\partial\psi}{\partial\rho} = \frac{1}{R}\left(\psi + \frac{\partial^2\psi}{\partial\theta^2}\right), \qquad \rho = R,\ \theta\in(0,2\pi) \qquad (11)
$$

where $\psi(\rho,\theta)$ indicate a generic test function.

The homogenized model here described is denoted with the acronym HOM in the foregoing.

2.3 Homogenized model for a imperfect rotor

The presence of imperfections can be accounted for in the homogenized model by letting the homogenized linear mass density and bending stiffness depend also on the angular variable θ. Accordingly, let assume that

$$
\overline{\sigma}_b(\rho,\theta) = \overline{\sigma}_{ob}(\rho) + \delta\overline{\sigma}_b(\rho,\theta), \qquad \overline{K}_b(\rho,\theta) = \overline{K}_{ob}(\rho) + \delta\overline{K}_b(\rho,\theta) \qquad (12)
$$

where $\delta\overline{\sigma}_b$ and $\delta\overline{K}_b$ are suitable perturbations superimposed to the homogenized nominal values of linear mass density $\overline{\sigma}_{ob}$ and bending stiffness $\overline{K}_{ob}$, respectively. In order to choose $\delta\overline{\sigma}_b$ and $\delta\overline{K}_b$ it is necessary to assume a specific behavior of the imperfect blades during the homogenization limit. To this end, for the sake of clarity, let assume that the j^{th} blade of the rotor has increased linear mass density equal to $\sigma_{ob} + \delta\sigma_{bj}$. It is assumed that when the number of blades is artificially increased to approach the homogenization limit, the number of imperfect blades is increased as well, as depicted in fig. 2; in doing so, the linear mass density and bending stiffness of the blades are rescaled according to the conditions given in section 2.2. In particular, if the number of blades is increased by a factor 2^n with n positive integer, the total number of blades becomes $N = 2^n N_b$ and the nominal value of the blade linear mass density rescales to $a = \sigma_{ob}/2^n$; the number of imperfect blades becomes $2^{n+1}-1$, equally spaced in the angular region centered in $\theta = \theta_j$, where the imperfect j^{th} blade is placed in the reference rotor, and whose amplitude is equal to the angular spacing $\delta\theta_o$ between two adjacent blades in the reference configuration; all the imperfect blades have rescaled linear mass density variation equal to $b = \delta\sigma_{bj}/2^n$, except the two blades at the boundary of this region, which have linear mass density variation $b/2$.

Under these assumptions it is easy to show that, in the homogenization limit $N\to\infty$, the homogenized linear mass density perturbation $\delta\overline{\sigma}_b$ and the homogenized bending stiffness perturbation $\delta\overline{K}_b$ are piecewise constant functions having the following expressions:

$$
\delta\overline{\sigma}_b(\rho,\theta) = \sum_{i=1}^{m}\frac{\delta\sigma_{bi}(\rho)}{\delta\theta_o}\chi_i(\theta), \qquad \delta\overline{K}_b(\rho,\theta) = \sum_{i=1}^{m}\frac{\delta K_{bi}(\rho)}{\delta\theta_o}\chi_i(\theta) \qquad (13)
$$

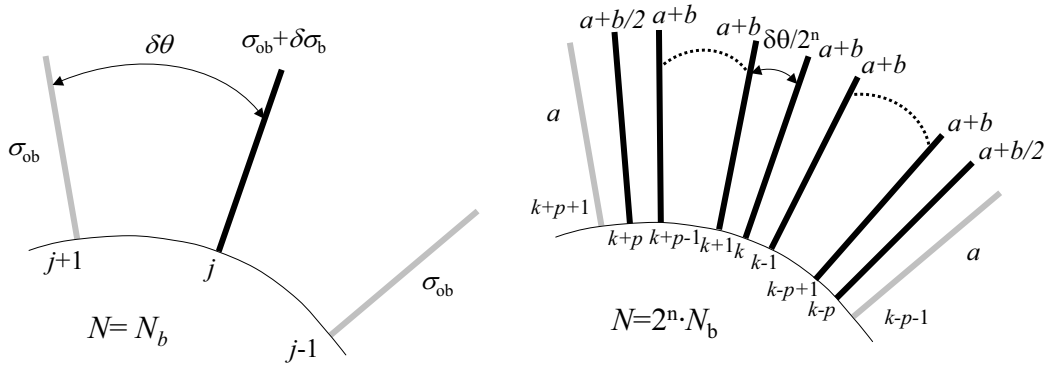

Figure 2: Homogenization limit for a imperfect rotor; imperfection due to the increase of linear mass density of a blade. On the left: reference rotor with N_b blades and imperfection on the j^{th} blade, in black color. On the right: rotor with $N = 2^n N_b$ blades with rescaled bending stiffness $K_{ob}/2^n$ and linear mass density $a = \sigma_{ob}/2^n$. Imperfect blades in black color; $k = 2^n(j-1)+1$, $p = 2^n - 1$, $b = \delta\sigma_{bj}/2^n$

.

where

$$\chi_i(\theta) = 1 \quad \forall\theta \in \left(\theta_i - \frac{\delta\theta_o}{2}, \theta_i + \frac{\delta\theta_o}{2}\right), \qquad \chi_i = 0 \quad \text{elsewhere} \tag{14}$$

3 ANALYTICAL SOLUTIONS FOR EIGENFREQUENCIES AND EIGENMODES

In this section explicit formulas for the evaluation of the eigenfrequencies and eigenmodes of a bladed rotor, with or without imperfections, are reported. They are obtained by using the homogenized model developed in sections. 2.2 and 2.3.

3.1 Perfect rotor

In order to evaluate the eigenmodes and eigenfrequencies of a perfect rotor by using the homogenized model here proposed, let assume for the sake of simplicity that $\overline{\sigma}_{ob}$ and $\overline{K}_{ob}$ do not depend on the radial variable ρ; under this simplifying assumption, using the localization lemma, equations (10) and (11) yields the field equilibrium equation:

$$-\omega^2\,\overline{\sigma}_{ob}U + \overline{K}_{ob}\frac{\partial^4 U}{\partial\rho^4} = 0, \qquad (\rho,\theta) \in (R, R+l_b)\times(0,2\pi) \tag{15}$$

and the boundary conditions:

$$
\begin{aligned}
&-\omega^2\sigma_r R\left(U-\frac{\partial^2 U}{\partial\theta^2}\right)+\omega^2\overline{\sigma}_{ob}l_b\frac{\partial^2 U}{\partial\theta^2}-\frac{K_r}{R^3}\left(\frac{\partial}{\partial\theta}+\frac{\partial^3}{\partial\theta^3}\right)^2 U\\
&\qquad\qquad -\frac{\overline{K}_{ob}}{R}\left(1+\frac{\partial^2}{\partial\theta^2}\right)\frac{\partial^2 U}{\partial\rho^2}-\overline{K}_{ob}\frac{\partial^3 U}{\partial\rho^3}=0 \qquad \rho=R,\ \theta\in(0,2\pi);\\
&\frac{\partial U}{\partial\rho}=\frac{1}{R}\left(U+\frac{\partial^2 U}{\partial\theta^2}\right) \qquad \rho=R,\ \theta\in(0,2\pi);\\
&\overline{K}_{ob}\frac{\partial^2 U}{\partial\rho^2}=0 \qquad \rho=R+l_b,\ \theta\in(0,2\pi);\\
&-\overline{K}_{ob}\frac{\partial^3 U}{\partial\rho^3}=0 \qquad \rho=R+l_b,\ \theta\in(0,2\pi).
\end{aligned}
\tag{16}
$$

Due to the rotational symmetry of the problem, the eigenmodes U depend harmonically on the angular variable θ. For each fixed nodal diameter, denoted by the modal number $n\geq 0$, a numerable set of eigenfrequencies and eigenmodes, denoted by the modal number $l=1,2,3\ldots$, can be computed as follows. Fixed n, a solution of the field equation (15) is given by

$$
U_{on,l}(\rho,\theta)=2A_{n,l}\left(\sum_{i=1}^{4}C_i\,f_i(\rho)\right)\cos(n\theta+\varphi_{n,l}) \tag{17}
$$

where $A_{n,l}$ is an arbitrary constant,

$$
\begin{aligned}
f_1(\rho)=\cos[\lambda_{n,l}(\rho-R)],\quad f_2(\rho)=\sin[\lambda_{n,l}(\rho-R)],\quad f_3(\rho)=\cosh[\lambda_{n,l}(\rho-R)],\\
f_4(\rho)=\sinh[\lambda_{n,l}(\rho-R)]
\end{aligned}
\tag{18}
$$

and the modal eigenfrequency $\omega_{on,l}$ is related to $\lambda_{n,l}$ by the relation

$$
\omega_{on,l}=\sqrt{\frac{\overline{K}_{ob}}{\overline{\sigma}_{ob}}}\lambda_{n,l}^2 \tag{19}
$$

In (17) the quantities $C_i,\ i=1\ldots4$ are scalar unknowns; by substituting (17) into the four boundary conditions (16) an eigenvalue problem is obtained, exhibiting a numerable set of eigenvalues $\lambda_{n,l}$, and corresponding eigenvectors $C_i,\ i=1\ldots4$. The phase orientation $\varphi_{n,l}$ is left undetermined after solving (15) and (16); as a consequence, for each fixed $n>0$ and l two independent eigenmodes exist, at the same modal frequency $\omega_{on,l}$. These are known in the literature as degenerate eigenmodes[Thomas, 1979, Shen, 1994]. All the eigenmodes relevant to $n=0$ are non-degenerate.

3.2 Linearized homogenized model for imperfect rotors

In order to derive analytical expressions for the modal eigenfrequencies and eigenmodes of rotor in the presence of imperfections, the homogenized model proposed in section 2.3 is linearized by performing an asymptotic expansion. Accordingly, the eigenmodes of the imperfect rotor are computed by perturbing the eigenmodes relevant to the perfect rotor, i.e., for each fixed couple of modal indices (n,l), the eigenmodes $U_{n,l}$ of the imperfect rotor are given by:

$$
U_{n,l}(\rho,\theta)=U_{on,l}(\rho,\theta)+\delta U_{n,l}(\rho,\theta) \tag{20}
$$

where $U_{on,l}$ is the eigenmode of the perfect rotor given in (17) and $\delta U_{n,l}$ is an unknown perturbation. Moreover the relevant eigenfrequency $\omega_{n,l}$ is given by

$$\omega_{n,l} = \omega_{on,l} + \delta\omega_{n,l} \tag{21}$$

where $\delta\omega_{n,l}$ is the frequency shift due to the presence of imperfections. By substituting the expansions (12), (20) and (21) into the weak formulation (10) and retaining only the first order terms, the following linearized weak formulation is obtained:

$$\begin{aligned}
&-\omega_{on,l}^2\Big\{\int_0^{2\pi}\sigma_r\left(\delta U_{n,l}\psi+\frac{\partial\delta U_{n,l}}{\partial\theta}\frac{\partial\psi}{\partial\theta}\right)\Big|_{\rho=R}R\,d\theta+\int_0^{2\pi}\int_R^{R+l_b}\overline{\sigma}_b\,\delta U_{n,l}\psi\,d\rho d\theta\\
&+\int_0^{2\pi}\overline{\sigma}_b l_b\frac{\partial\delta U_{n,l}}{\partial\theta}\frac{\partial\psi}{\partial\theta}\Big|_{\rho=R}d\theta\Big\}+\int_0^{2\pi}\frac{K_r}{R^4}\left(\frac{\partial\delta U_{n,l}}{\partial\theta}+\frac{\partial^3\delta U_{n,l}}{\partial\theta^3}\right)\left(\frac{\partial\psi}{\partial\theta}+\frac{\partial^3\psi}{\partial\theta^3}\right)\Big|_{\rho=R}R\,d\theta\\
&+\int_0^{2\pi}\int_R^{R+l_b}\overline{K}_b\frac{\partial^2\delta U_{n,l}}{\partial\rho^2}\frac{\partial^2\psi}{\partial\rho^2}\,d\rho d\theta=2\omega_{on,l}\delta\omega_{n,l}\Big\{\int_0^{2\pi}\sigma_r\left(U_{on,l}\psi+\frac{\partial U_{on,l}}{\partial\theta}\frac{\partial\psi}{\partial\theta}\right)\Big|_{\rho=R}R\,d\theta\\
&+\int_0^{2\pi}\int_R^{R+l_b}\overline{\sigma}_b U_{on,l}\psi\,d\rho d\theta+\int_0^{2\pi}\overline{\sigma}_b l_b\frac{\partial U_{on,l}}{\partial\theta}\frac{\partial\psi}{\partial\theta}\Big|_{\rho=R}d\theta\Big\}+\omega_{on,l}^2\Big\{\int_0^{2\pi}\int_R^{R+l_b}\delta\overline{\sigma}_b\,U_{on,l}\psi\,d\rho d\theta\\
&+\int_0^{2\pi}l_b\,\delta\overline{\sigma}_b\frac{\partial U_{on,l}}{\partial\theta}\frac{\partial\psi}{\partial\theta}\Big\}-\int_0^{2\pi}\int_R^{R+l_b}\delta\overline{K}_b\frac{\partial^2U_{on,l}}{\partial\rho^2}\frac{\partial^2\psi}{\partial\rho^2}\,d\rho d\theta
\end{aligned}\tag{22}$$

under the constraints

$$\frac{\partial\delta U_{on,l}}{\partial\rho}=\frac{1}{R}\left(\delta U_{on,l}+\frac{\partial^2\delta U_{on,l}}{\partial\theta^2}\right),\quad \frac{\partial\psi}{\partial\rho}=\frac{1}{R}\left(\psi+\frac{\partial^2\psi}{\partial\theta^2}\right),\quad \rho=R,\ \theta\in(0,2\pi) \tag{23}$$

where it is assumed, for simplicity, that $\overline{\sigma}_{ob}$ and $\overline{K}_{ob}$ do not depend on the radial variable ρ. The unknowns appearing in (22) are the scalar quantities $\delta\omega_{n,l}$, $\varphi_{n,l}$ and the function $\delta U_{n,l}$. Due to the presence of the imperfections, the indeterminacy on the phase angle $\varphi_{n,l}$ is removed and, for each couple of modal indexes (n,l), two set of solutions $(\delta\omega_{n,l},\varphi_{n,l},\delta U_{n,l})$ are expected to be found, corresponding to the two split eigenmodes belonging to the same degenerate eigenmode $U_{on,l}$ relevant to the perfect structure. This linearized homogenized model is denoted in the foregoing with the acronym L-HOM.

3.3 Eigenfrequencies and eigenmodes evaluation for a imperfect rotor

In order to derive analytical expressions for the split eigenfrequencies and eigenmodes of an imperfect rotor, the linearized variational formulation (22) is here adopted. It is observed that, for each fixed modal number n,

$$\begin{aligned}
g_1(\rho,\theta) &= \left(\sum_{i=1}^4 C_i f_i(\rho)\right)\cos(n\theta)\\
g_2(\rho,\theta) &= \left(\sum_{i=1}^4 C_i f_i(\rho)\right)\sin(n\theta)
\end{aligned}\tag{24}$$

with C_i, $i=1\dots4$ and $\lambda_{n,l}$ solutions of (15) and (16), are two independent functions belonging to the kernel of the self-adjoint operator in (22). Accordingly, by substituting once $\psi=g_1$ and then

$\psi = g_2$ in (22), together with the expression of $U_{on,l}$ given by (17), two independent equations in the unknowns $\delta\omega_{n,l}$ and $\varphi_{n,l}$ are obtained, whose solutions supply the two couples of frequency split and phase orientation $(\delta\omega_{n,l}, \varphi_{n,l})$ relevant to the perturbed mode (n,l). Once the values of $\delta\omega_{n,l}$ and $\varphi_{n,l}$, in correspondence of a choice of modal numbers (n,l), have been computed, the corresponding modal shapes can be obtained by making use of the linear weak formulation (22). To this end (22) is integrated by parts with respect to the variable ρ and, making use of the first of (23), it yields

$$\begin{aligned}
&\int_0^{2\pi}\int_R^{R+l_b}\Big(-\omega_{on,l}^2\overline{\sigma}_b\delta U_{n,l}+\overline{K}_b\frac{\partial^4\delta U_{n,l}}{\partial\rho^4}-2\omega_{on,l}\delta\omega_{n,l}\overline{\sigma}_b U_{on,l}-\omega_{on,l}^2\delta\overline{\sigma}_b U_{on,l}\\
&+\delta\overline{K}_b\frac{\partial^4 U_{n,l}}{\partial\rho^4}\Big)\psi\,d\rho d\theta+\int_0^{2\pi}\Big\{-\omega_{on,l}^2\sigma_r R\left(\delta U_{n,l}\psi+\frac{\partial\delta U_{n,l}}{\partial\theta}\frac{\partial\psi}{\partial\theta}\right)-\omega_{on,l}^2\overline{\sigma}_b l_b\frac{\partial\delta U_{n,l}}{\partial\theta}\frac{\partial\psi}{\partial\theta}\\
&+\frac{K_r}{R^3}\left(\frac{\partial\delta U_{n,l}}{\partial\theta}+\frac{\partial^3\delta U_{n,l}}{\partial\theta^3}\right)\left(\frac{\partial\psi}{\partial\theta}+\frac{\partial^3\psi}{\partial\theta^3}\right)-\frac{\overline{K}_b}{R}\frac{\partial\delta U_{n,l}}{\partial\rho^2}\left(\psi+\frac{\partial^2\psi}{\partial\theta^2}\right)+\overline{K}_b\frac{\partial^3\delta U_{n,l}}{\partial\rho^3}\psi\\
&-2\omega_{on,l}\delta\omega_{n,l}\left[\sigma_r R\left(U_{on,l}\psi+\frac{\partial U_{on,l}}{\partial\theta}\frac{\partial\psi}{\partial\theta}\right)+\overline{\sigma}_b l_b\frac{\partial U_{on,l}}{\partial\theta}\frac{\partial\psi}{\partial\theta}\right]-\omega_{on,l}^2 l_b\delta\overline{\sigma}_b\frac{\partial U_{on,l}}{\partial\theta}\frac{\partial\psi}{\partial\theta}\\
&-\frac{\delta\overline{K}_b}{R}\frac{\partial^2 U_{on,l}}{\partial\rho^2}\left(\psi+\frac{\partial^2\psi}{\partial\theta^2}\right)+\delta\overline{K}_b\frac{\partial^3 U_{on,l}}{\partial\rho^3}\psi\Big\}\Big|_{\rho=R}d\theta+\int_0^{2\pi}\Big[\Big(\overline{K}_b\frac{\partial^2\delta U_{n,l}}{\partial\rho^2}\\
&+\delta\overline{K}_b\frac{\partial^2 U_{on,l}}{\partial\rho^2}\Big)\frac{\partial\psi}{\partial\rho}\Big]_{\rho=R+l_b}d\theta+\int_0^{2\pi}\left[\left(-\overline{K}_b\frac{\partial^3\delta U_{n,l}}{\partial\rho^3}-\delta\overline{K}_b\frac{\partial^2 U_{on,l}}{\partial\rho^3}\right)\psi\right]_{\rho=R+l_b}d\theta=0
\end{aligned}\tag{25}$$

Another weak-form equation is obtained multiplying the second of (23) by ψ and integrating over $(0, 2\pi)$, which reads as:

$$\int_0^{2\pi}\left[\frac{\partial\delta U_{n,l}}{\partial\rho}-\frac{1}{R}\left(\delta U_{on,l}+\frac{\partial^2\delta U_{n,l}}{\partial\theta^2}\right)\right]\psi\,d\theta=0 \tag{26}$$

In order to find out the unknown modal perturbation $\delta U_{n,l}$, a spectral representation is used by setting

$$\delta U_{n,l}(\rho,\theta)=\sum_{i=1}^{4}\left\{\frac{C_{i0}}{2}+\rho\frac{G_{i0}}{2}+\sum_{k>0}\left[(C_{ik}+\rho G_{ik})\cos(k\,\theta)+(D_{ik}+\rho H_{ik})\sin(k\,\theta)\right]\right\}f_i(\rho) \tag{27}$$

The representation (27) of $\delta U_{n,l}$ is then substituted in (25), and the test function ψ is chosen according to the following expressions

$$\psi(\rho,\theta)=\cos(k\theta)\beta(\rho),\qquad \psi(\rho,\theta)=\sin(k\theta)\beta(\rho) \tag{28}$$

where k is any positive fixed integer and β is an arbitrary function of ρ. Using the localization lemma in the first integral of (25) an explicit expression for G_{ik} and H_{ik}, $i = 1\ldots4$ is obtained. The expression (27) for $\delta U_{n,l}$, where now G_{ik} and H_{ik} are known scalar quantities, is then substituted into (25) and (26). Linear equations in the unknown coefficients C_{ik} and D_{ik} are obtained, for each fixed positive integer k, by choosing the test function ψ and $\partial\psi/\partial\theta$, at $\rho = R$ and $\rho = R + l_b$, as $\cos(k\,\theta)$ and $\sin(k\,\theta)$ and using again localization lemma. Their solution provides the Fourier coefficients of the unknown modal perturbation $\delta U_{n,l}$.

4 NUMERICAL SIMULATIONS

In this section some numerical simulation results are presented, in order to show the effectiveness of the proposed homogenized model in the investigation of the frequency split and localization phenomenon in imperfect rotors.

4.1 Case study bladed rotor

A case study problem is here introduced; a bladed rotor, similar to the one schematically represented in fig. 1, is considered. It is composed of 32 elastic blades of cross section $2 \times 50\,\text{mm}$ and length $600\,\text{mm}$; the blades are clamped to a support ring of radius $200\,\text{mm}$ and cross section $4 \times 50\,\text{mm}$. The ring and the blades are comprised of steel, with Young modulus $210\,\text{GPa}$ and mass density $7850\,\text{Kg/m}^3$. The degenerate modal frequencies of this bladed rotor are reported in table 1, relevant to modal numbers $n = 2, \dots 5$ and $l = 1$ and evaluated according to the EB model.

$n=2$		$n=3$		$n=4$		$n=5$	
27.0746	27.0746	27.9718	27.9718	28.4242	28.4242	28.6596	28.6596

Table 1: Modal frequencies $\omega_{on,l}$ in rad/s, relevant to the perfect rotor and evaluated according to the EB model. Modal frequencies relevant to modal numbers $n = 2$, $n = 3$, $n = 4$, $n = 5$ and $l = 1$

4.2 Numerical algorithms

In this section several numerical algorithms are briefly described, in order to find a minimizer for the Hamiltonian functional (2), describing the dynamical behavior of the case study bladed rotor, and to solve the variational equation (10), describing the dynamical behavior of the homogenized bladed rotor. The functional (2) is discretized by using two-node beam elements and Hermite polynomials as interpolation scheme, both for the ring and the blades. The axial inextensibility constraint is enforced by using a penalization method. A discrete formulations for the dynamical problem is finally obtained by assuming as unknowns the nodal displacements and rotations.

The homogenized weak formulation in (10), defined in the annular region $(R, R + l_b) \times (0, 2\pi)$, is discretized in the angular direction with the Ritz-Rayleigh method assuming, as shape functions,

$$1, \quad 2\cos(k\theta), \quad -2\sin(k\theta) \qquad k = 1, 2, \dots n_f \tag{29}$$

whereas a finite element discretization is assumed in the radial direction, employing two-node beam elements with Hermite polynomials as interpolation scheme. Accordingly, the nodal unknowns are the real and imaginary part of the complex Fourier coefficients of the tangential displacement U and its radial derivative.

4.3 Validation of the homogenization limit

In this section the homogenization limit is numerically studied, and a convergence analysis is presented. The modal eigenfrequencies of the perfect rotor described in section 4.1 are computed increasing the number N of blades, starting from the reference configuration with 32 blades, and rescaling at the same time the linear mass density and the bending stiffness of the blades as described in section 2, in order to approach the homogenization limit $N \to \infty$ relevant to the HOM model. In particular, $N = 32$, $N = 64$, $N = 128$ and $N = 256$ have been considered in the computations. In fig. 3 the relative error between degenerate eigenfrequencies evaluated according to the EB model and the HOM model are reported, relevant to modal numbers $n = 2, \dots 5$ and $l = 1$. The figure

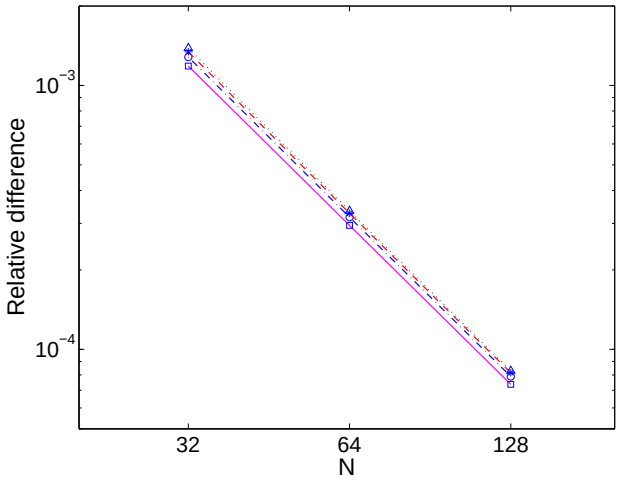

Figure 3: Convergence analysis for the homogenization limit: relative error between modal frequencies evaluated according to the EB model and according to the HOM model, as a function of the number of blades N. Rotor without imperfections. Modal frequencies relevant to modal numbers $\square$ $n = 2, l = 1$; $\circ$ $n = 3, l = 1$; $*$ $n = 4, l = 1$; $\triangle$ $n = 5, l = 1$

shows that a quadratic convergence to the homogenized solution is achieved. The relative error slightly increases with the increase of n. The homogenized model turns out to be quite accurate in describing the rotor dynamics, as the relative error is very small even in the reference case of 32 blades.

4.4 Modal frequency analysis

In this section the modal frequencies relevant to an imperfect bladed rotor are analyzed. The imperfection is introduced by increasing the linear mass density of fourth blade of the perfect rotor described in section 4.1 by a factor γ. The modal frequencies $\omega_{n,l}$, relevant to modal numbers $n = 2, \dots 5$ and $l = 1$, are evaluated according to the EB model and the HOM model, considering different values of γ. In table 2 the modal frequencies evaluated according to the EB model are reported.

	$n=2$		$n=3$		$n=4$		$n=5$	
$\gamma = 0.0005$	27.0742	27.0746	27.9713	27.9718	28.4237	28.4242	28.6591	28.6596
$\gamma = 0.001$	27.0738	27.0746	27.9709	27.9718	28.4233	28.4242	28.6587	28.6596
$\gamma = 0.005$	27.0703	27.0746	27.9671	27.9718	28.4193	28.4242	28.6544	28.6596
$\gamma = 0.01$	27.0656	27.0746	27.9619	27.9718	28.4134	28.4242	28.6476	28.6596

Table 2: Modal frequencies $\omega_{n,l}$ in rad/s, relevant to the imperfect rotor and evaluated according to the EB model. The imperfection is introduced by increasing the mass of the fourth blade of the perfect rotor described in section 4.1 by a factor $\gamma = 0.0005, 0.001, 0.005, 0.01$, with respect to its nominal value. Modal frequencies relevant to modal numbers $n = 2$, $n = 3$, $n = 4$, $n = 5$ and $l = 1$

From table 2 it can be seen that, due to the presence of imperfections, a frequency split occurs

between frequencies belonging to the same modal number (n, l), which where coinciding in the perfect case as shown in table 1. The difference between eigenfrequencies relevant to the imperfect rotor in table 2 and the corresponding ones relevant to the perfect rotor in table 1 is the frequency shift $\delta\omega_{n,l}$ which occurs due to the presence of imperfections. In particular, due to the particular choice of the imperfection, for each couple of modal numbers (n, l) one of the two frequency shifts $\delta\omega_{n,l}$ is vanishing; in fact, for each fixed (n, l), one of the two eigenfrequencies of the imperfect rotor in table 2 coincides with the corresponding frequency of the perfect rotor in table 1. A similar result is obtained in [Fang et al., 2006]. Table 3 contains the relative error between the frequency shifts $\delta\omega_{n,l}$ evaluated according to the EB model and to the HOM model, relevant to the same imperfect bladed rotor. For each couple of modal numbers (n, l) only one value is reported, relevant to the non vanishing frequency shifts. The errors are almost independent from the imperfection coefficient γ,

	$n = 2$	$n = 3$	$n = 4$	$n = 5$
γ=0.0005	0.0114	0.0281	0.0513	0.0824
γ=0.001	0.0116	0.0283	0.0519	0.0834
γ=0.005	0.0125	0.0299	0.0556	0.0906
γ=0.01	0.0103	0.0261	0.0500	0.0828

Table 3: Relative error between frequency shifts relevant to the imperfect rotor, evaluated according to the HOM model and the EB model. The imperfection is introduced by increasing the mass of the fourth blade of the perfect rotor described in section 4.1 by a factor $\gamma = 0.0005, 0.001, 0.005, 0.01$, with respect to its nominal value. Modal frequencies relevant to modal numbers $n = 2$, $n = 3$, $n = 4$, $n = 5$ and $l = 1$

and they slightly increase with the increase of n, ranging from 1% when $n = 2$ to 9% when $n = 5$. Finally, in table 4 the relatives errors between frequency shifts $\delta\omega_{n,l}$ evaluated according to the HOM model and the L-HOM model are reported. For each couple of modal numbers (n, l) only one value is reported, relevant to the relative error between the non vanishing frequency shifts. Results

	$n = 2$	$n = 3$	$n = 4$	$n = 5$
$\gamma = 0.0005$	0.0032	0.0054	0.0087	0.0125
$\gamma = 0.001$	0.0064	0.0108	0.0173	0.0250
$\gamma = 0.005$	0.0319	0.0539	0.0860	0.1233
$\gamma = 0.01$	0.0665	0.1122	0.1777	0.2507

Table 4: Relative error between frequency shifts relevant to the imperfect rotor, evaluated according to the HOM model and the L-HOM model. The imperfection is introduced by increasing the mass of the fourth blade of the perfect rotor described in section 4.1 by a factor $\gamma = 0.0005, 0.001, 0.005, 0.01$, with respect to its nominal value. Modal frequencies relevant to modal numbers $n = 2$, $n = 3$, $n = 4$, $n = 5$ and $l = 1$

in table 4 show that the linearized model is suitable for accurately evaluating frequency shifts of a imperfect rotor when imperfections are sufficiently small; for $\gamma \leq 0.001$ the relative errors ranges from 0.3% to 2.5%, increasing with mode number n. The relative difference between frequency shifts becomes larger for larger values of γ together with higher values of mode number n; for an increased accuracy a refined theory may be used, obtained by retaining in the perturbation expansion performed in section 3.2 also the higher order infinitesimal terms. Accordingly a non linear theory

would be obtained, whose solution would require a numerical iterative procedure.

4.5 Eigenmode analysis

In this section the eigenmodes of the rotor described in section 4.1, made imperfect by increasing the linear mass density of its 4^{th} blade by a factor $\gamma = 0.01$, are evaluated. For the sake of comparison both the HOM model and the L-HOM model are employed in the analysis. In fig. 4 the eigenmodes relevant to mode numbers $n = 2, 3, 4, 5$ and $l = 1$ are reported; in particular, for each couple of modal number (n, l) only the eigenmode corresponding to a non vanishing frequency shift $\delta\omega_{n,l}$ exhibits a vibration localization and appears in the figure. The modal shapes relevant to the perfect rotor are with blue dashed line, the modal shapes relevant to the imperfect ring and evaluated with the L-HOM model are reported with continuous green line whereas the red mixed line refers to the modal shapes relevant to the imperfect ring and evaluated using the HOM model. All the modal shapes have been normalized using the same procedure; they have been rescaled in such a way as to make the modulus of the complex Fourier coefficient relevant to the dominant mode (i.e. the $n^{th} + 1$ Fourier coefficient for a eigenmode of mode number n) equal to 1. Finally, the eigenmodes have been rescaled by a factor 0.2 before being represented in the figure.

The homogenized model turns out to be suitable for studying the localization phenomenon in imperfect rotors: in fact, as shown in fig. 4, the localization effect due to the imperfection placed on the fourth blade clearly appears, increasing with the increase of the modal number n. It turn out that the HOM model and the L-HOM model are in close agreement for evaluating the modal shapes, with the L-HOM model slightly underestimating the modal amplitude around the imperfect blade with respect to the HOM model.

5 Conclusions

In this paper a homogenized model has been proposed, suitable for the analysis of the frequency split and vibration localization phenomenon in imperfect bladed rotors. The model seems to be a good compromise between accuracy and simplicity; indeed it considers the coupling between a single blade and all the other ones, due to the presence of the support disk. On the other end, it is a continuous model and thus it is synthetic and computationally more efficient than classical finite element models. Numerical simulations reported show its ability in studying the frequency split and vibration localization phenomenon. The proposed model may be an efficient tool for the design and the parametric analysis of turbine machineries and rotationally periodic structures in general.

References

[Cai et al., 1990] Cai, C. W., Cheung, Y. K., and Chan, H. (1990). Uncoupling of dynamic equations for periodic structures. *J. Sound Vib.*, 139:253–273.

[Chiu and Huang, 2007] Chiu, Y. J. and Huang, S. C. (2007). The influence on coupling vibration of a rotor system due to a mistuned blade length. *Int. J. Mech. Sci.*, In press.

[Fang et al., 2006] Fang, X., Tang, J., Jordan, E., and Murphy, K. D. (2006). Crack induced vibration localization in simplified bladed-disk structures. *J. Sound Vib.*, 291:395–418.

[Fricker and Potter, 1981] Fricker, A. J. and Potter, S. (1981). Transient forced vibration of rotationally periodic structure. *Int. J. Numer. Meth. Eng.*, 17:957–974.

[Huang, 2006] Huang, B. W. (2006). Effect of numbers of blades and distribution of cracks on vibration localization in a cracked pre-twisted blade system. *Int J. Mech. Sci.*, 48:1–10.

[Pierre and Dowell, 1987] Pierre, C. and Dowell, E. H. (1987). Localization of vibration by structural irregularity. *J. Sound Vib.*, 114(3):549–564.

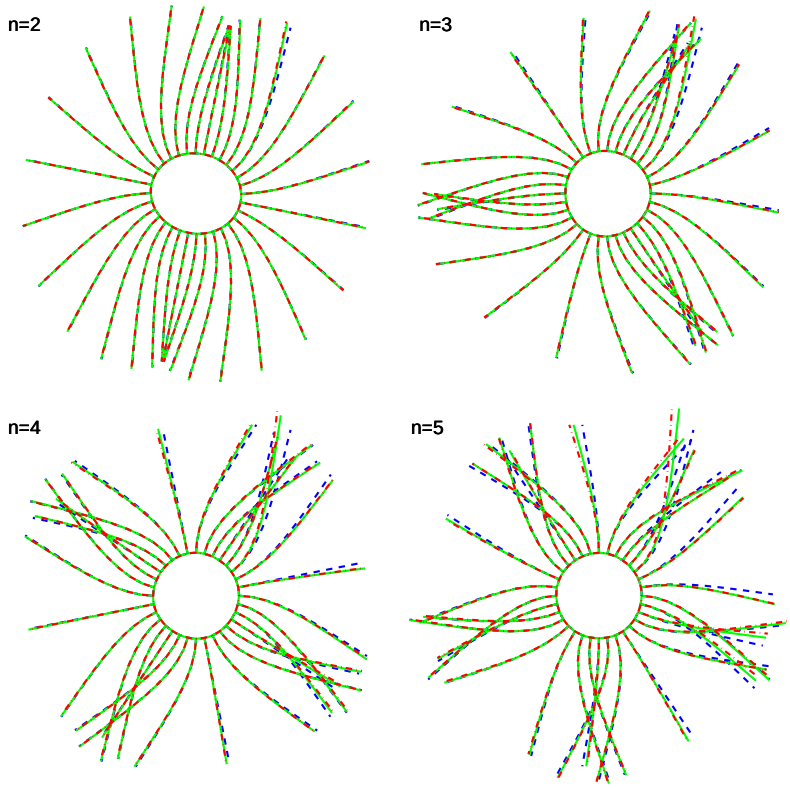

Figure 4: Eigenmodes of the imperfect rotor, evaluated according to the HOM model and the L-HOM model. The imperfection is introduced by increasing the mass of the fourth blade of the perfect rotor described in section 4.1 by a factor $\gamma = 0.01$, with respect to its nominal value. $--$ blue: perfect rotor, — green: imperfect rotor using L-HOM model, $- \cdot -$ red: imperfect rotor using HOM model.

[Shen, 1994] Shen, I. Y. (1994). Vibration of rotationally periodic structures. *J. Sound Vib.*, 172:459–470.

[Sinha, 1986] Sinha, A. (1986). Calculating the statistics of forced response of a mistuned bladed disk assembly. *AIAA J.*, 24:1797–1801.

[Tang and Wang, 2003] Tang, J. and Wang, K. W. (2003). Vibration delocalization of nearly periodic structures using coupled piezoelectric networks. *J. Vib. Acoust.*, 125:95–108.

[Thomas, 1979] Thomas, D. L. (1979). Dynamics of rotationally periodic structures. *Int. J. Numer. Meth. Eng.*, 14:81–102.

[Wagner and Griffin, 1993] Wagner, L. F. and Griffin, J. (1993). A continuous analog model for grouped-blade vibration. *J. Sound Vib.*, 165:421–438.

[Yoo et al., 2003] Yoo, H. H., Kim, J. Y., and Inman, D. J. (2003). Vibration localization of simplified mistuned cyclic structures undertaking external harmonic force. *J. Sound Vib.*, 261:859–870.